Available online at www.sciencedirect.com
SCIENCE DIRECT®
Journal of Solid State Chemistry 179 (2006) 2732–2738
JOURNAL OF SOLID STATE CHEMISTRY
www.elsevier.com/locate/jssc

Rapid communication

"Unusual" phase transitions in $CeAlO_3$

W.T. Fu*, D.J.W. IJdo

Leiden Institute of Chemistry, Gorlaeus Laboratories, Leiden University, P.O. Box 9502, 2300 RA Leiden, The Netherlands

Received 6 February 2006; received in revised form 21 April 2006; accepted 5 May 2006
Available online 13 May 2006

Abstract

High-resolution time-of-flight neutron powder diffraction was carried out to investigate the crystal structures of $CeAlO_3$ over a wide temperature range between 4.2 and 1423 K. Confirming the recent result of X-ray powder diffraction, the room temperature structure is tetragonal with the space group $I4/mcm$ (tilt system ($a^0a^0c^-$)). The tetragonal structure persists down to 4.2 K. However, above room temperature $CeAlO_3$ undergoes three phase transitions: first to the orthorhombic *Imma* structure (tilt system ($a^0b^-b^-$)) at, e.g., 373 K, then to the rhombohedral $R\bar{3}c$ structure (tilt system ($a^-a^-a^-$)) at, e.g., 473 K, and finally, to the primitive cubic $Pm\bar{3}m$ structure which exists above 1373 K. The sequence of phases, $Pm\bar{3}m \rightarrow R\bar{3}c \rightarrow Imma \rightarrow I4/mcm$, which occurs in $CeAlO_3$ is a rare one in oxide perovskites.

Keywords: Perovskites; Neutron powder diffraction; Crystal structure; Phase transition

1. Introduction

In recent years there has been a renewed interest in the problem of the phase transitions in perovskites. Many ABO_3 oxide perovskites at room temperature or below have structures which are distorted from the ideal cubic aristotype. The distortion mostly occurs when the ionic radii, r_A, r_B and r_O, do not fulfil the condition for the Goldsmith tolerance factor, $t = 1$, $t = (r_A + r_O)/\sqrt{2}(r_B + r_O)$. Generally, based on t two mechanisms of distortion may be distinguished[1]: A *B*-cation driven one ($t > 1$) and one driven by the *A*-cation ($t < 1$). In the first case, the *B*-cation is nominally too small for its octahedral site, tending to move from the centre. This type of distortion typically results in ferro-electricity as in tetragonal $BaTiO_3$ [1]. Conversely, when $t < 1$, the cubic cavity formed by corner-linked BO_6 octahedra is too large for *A*, consequently the minimum energy distortion mode is realised by tilting the normally rigid BO_6 octahedra. In such cases, the *A*–O distances are shortened while the first coordination sphere of the *B*-cation remains virtually unchanged, only the soft *B*–O–*B* angle being disturbed. Between the two distortion mechanisms, the *A*-cation driven one is the most common. In particular, as there are many different ways of tilting the BO_6 octahedra, in practice this type of distortion results in many different structures. Glazer [2,3] analysed the different tilting patterns in terms of component tilts around the three cubic axes, obtaining 23 tilt systems. He also introduced a convenient symbolic description ($a^{\pm}b^{\pm}c^{\pm}$) which is now universally adopted. Here the symbols indicate the tilting magnitudes about the given axis and "+" and "−" represent whether the adjacent octahedral layer is tilted in phase or out of phase. Although Glazer's classification of the tilt systems may be very helpful in describing the structure of distorted perovskites, it provides no information on what would be the logical phase sequence in the case of a particular perovskite in a changing environment. Recently, Howard and Stokes [4] have, based on group theoretical considerations, re-analysed the problem of octahedral tilting in simple perovskites. They have listed 15 possible space groups covering all possible tilt systems. They also presented a diagram of the group–subgroup relationships and the nature of the corresponding phase

*Corresponding author. Tel.: +31 71 5274215; fax: +31 71 5274537.
E-mail address: w.fu@chem.leidenuniv.nl (W.T. Fu).

[1]Distortion from cubic symmetry in perovskites may be due to Jahn–Teller effect caused by the *B*-cation, for instance if *B* is Mn(III) or Cu(II).

0022-4596/$ - see front matter © 2006 Elsevier Inc. All rights reserved.
doi:10.1016/j.jssc.2006.05.002

transitions, i.e., being either discontinuous or possibly continuous.

Among the recently studied phase transitions in ABO_3 perovskites, two transition pathways have been well established. In $SrZrO_3$ [5,6], $SrHfO_3$ [7], $SrRuO_3$ [8,9] and $BaTbO_3$ [10], the sequence on decreasing temperature, is $Pm\bar{3}m \rightarrow I4/mcm \rightarrow Imma \rightarrow Pnma$, though the *Pnma* structure does not occur in $BaTbO_3$. In $BaCeO_3$ [11], the sequence is $Pm\bar{3}m \rightarrow R\bar{3}c \rightarrow Imma \rightarrow Pnma$. Other phase sequences such as $Pm\bar{3}m \rightarrow I4/mcm \rightarrow Imma \rightarrow I2/m$ or $Pm\bar{3}m \rightarrow R\bar{3}c \rightarrow Imma \rightarrow I2/m$ have also been reported for $BaPbO_3$ [12,13] and $PrAlO_3$ [14,15], respectively. However, a recent high-resolution time-of-flight neutron powder diffraction study has ruled out the existence of the $I2/m$ structure in $BaPbO_3$ [16].

The lanthanide ortho-aluminates, $LnAlO_3$ (Ln = lanthanides and Y), have long been known to be distorted perovskites. At room temperature, two structures have been well determined previously. For large lanthanides, i.e., Ln = La, Pr and Nd, the structure is rhombohedral with the space group $R\bar{3}c$ (tilt system ($a^-a^-a^-$)) [17–19]. With smaller lanthanides (Ln = Sm–Lu and Y), $LnAlO_3$ are of the orthorhombic $GdFeO_3$-type structure, having the space group *Pnma* (tilt system ($a^+b^-b^-$)) [18,20–23].

Among the lanthanide ortho-aluminates the structure of $CeAlO_3$ is of a particular interest as it is reported to have a different symmetry than the neighbouring $LaAlO_3$ and $PrAlO_3$ at room temperature. Moreover, the formation of this compound was known to remarkably stabilise the high-surface γ-Al_2O_3 in current three-way catalyst systems [24]. Zachariasen [25] and Tas and Akinc [26] found a tetragonal cell for $CeAlO_3$ with the lattice parameters closely related to that of the cubic aristotype (a_p) ($a \approx 3.77$ Å and $c \approx 3.79$ Å), though Roth [27] and Kim [28] described it as rhombohedral ($a = 5.327$ Å and $\alpha = 60.25°$). Leonov et al. [29] have studied the Ce_2O_3–Al_2O_3 system, and reported the binary phase diagram. They showed two phase transitions in $CeAlO_3$ at 363 and 1253 K. However, this result has not been confirmed by Tas and Akinc [26] in their DTA analysis of $CeAlO_3$. On the other hand, Egorov et al. [30] carried out differential scanning calorimetry measurements on $CeAlO_3$ in the temperature range 300–800 K, demonstrating the presence of two phase transitions at 310 and 450 K, respectively. Shelykh and Melekh [31] have studied the electrical and optical properties of single crystals of $CeAlO_3$, confirming the phase transitions reported by Egorov et al. [30]. They also observed a decrease of optical transmittance starting at 1170 K and completing at 1400 K, which was attributed to the transition to an isotropic cubic phase. In these papers no structural details were given. The structure of $CeAlO_3$ at room temperature has been determined by Tanaka et al. [32] from their X-ray single crystal diffraction data. They confirmed the presence of a primitive tetragonal cell and refined the structure in the space group $P4/mmm$. However, the tetragonal distortion in $CeAlO_3$ cannot simply be explained in a primitive cell without considering the electronic instability, e.g., *B*-cation displacement or Jahn–Teller distortion. In addition, the space group $P4/mmm$ does not occur in any of the pathways derived by Glazer [2–4]. Considering further that the basal oxygen atoms of the AlO_6 octahedron showed remarkably non-spherical distribution of the electron density when modelled in $P4/mmm$ [32], the choice of a primitive cell for $CeAlO_3$ seems to be inappropriate.

Recently, we re-examined [33] the crystal structure of $CeAlO_3$ using X-ray powder diffraction data. From the presence of a few very weak but nevertheless clearly visible super lattice reflections, we ruled out the possibility of a primitive cell and modelled the structure with a super cell, $a \approx \sqrt{2}a_p$ and $c \approx 2a_p$, in the space group $I4/mcm$, (tilt system ($a^0a^0c^-$)) [2–4]. Given that the ionic radius of Ce^{3+} is just in-between those of La^{3+} and Pr^{3+}, the occurrence of the $I4/mcm$ structure is quite unexpected. In particular, from the phase transitions observed thus far, one might anticipate $CeAlO_3$ crystallising in $Pm\bar{3}m$ at high temperatures, turning into *Imma* and possibly *Pnma* ($I2/m$) on cooling. This would exclude the possible existence of the rhombohedral $R\bar{3}c$ structure for $CeAlO_3$, observed in the neighbouring $LaAlO_3$ and $PrAlO_3$. To clear this matter up once and for all we carried out a high-resolution time-of-flight neutron powder diffraction study on $CeAlO_3$ between 4.2 and 1423 K. In this paper we report the phase sequence observed.

2. Experimental

A sample of $CeAlO_3$ (~5 g) was prepared from high-purity CeO_2 (99.999%) and Al_2O_3 (99.99%) in a platinum crucible. The stoichiometric mixtures were ground intimately and fired in a flow of diluted hydrogen (10% H_2 in N_2) at 1773 K for 24 h. After regrinding this treatment was repeated twice, whereupon the reaction mixture was allowed to cool to room temperature.

X-ray powder diffraction was used to check the sample's purity. High-resolution time-of-flight powder neutron diffraction data were collected on the HRPD diffractometer at the ISIS Facility, Rutherford Appleton Laboratories. The sample was loaded into an 11 mm diameter vanadium can and mounted either in a cryostat ($T \leqslant 300$ K) or in a furnace ($T > 300$ K). Measurements were carried out in vacuo (~10^{-6} Torr). Before a measurement was started the sample was kept at the specific temperature for about 10 min to allow thermal equilibrium to occur. During data collection, the temperature fluctuation is approximately ± 0.5 °C. The diffraction patterns were recorded in both the backscattering bank and the 90° detector bank, over the time-of-flight range 32–120 and 35–114 ms, corresponding to *d*-spacings ranging from 0.6 to 2.5 Å and 1.0 to 3.3 Å, respectively. The patterns were normalised to the incident beam spectrum as recorded in the upstream monitor, and corrected for detector efficiency according to a prior calibration with vanadium (rod). Most patterns were recorded to a total incident proton beam of about

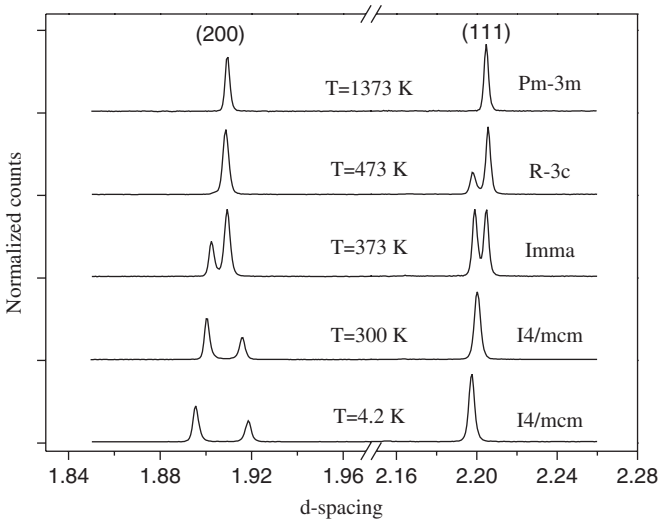

Fig. 1. A section of the high-resolution backscattering data showing the evolution of the basic (1 1 1) and (200) reflections as the function of temperature. The significance of the peak splitting and the change of their relative intensities is discussed in the text.

30 μAh, in approximately 2 h. Calculations were performed simultaneously on both backscattering and 90° bank data by the Rietveld method using the GSAS computer program [34].

3. Results

Confirming our earlier X-ray diffraction study [33], the high-resolution backscattering data of $CeAlO_3$ at room temperature demonstrates the presence of a super cell, easily identified from the substantial intensity of the superlattice reflections. Tetragonal symmetry is identified by examination of the peak splitting of the basic reflections of the cubic perovskite, i.e., the (*h*00)-type reflections are split into doublets and the (*hhh*)-type reflections remain single (Fig. 1). As no additional reflections associated with in-phase tilting of adjacent octahedra are present, the logical choice of the space group is *I*4/*mcm* [4]. Below room temperature no structural change was observed except an increasing tetragonal distortion (Fig. 1). Therefore, the structure of $CeAlO_3$ between 4.2 and 300 K was modelled in the space group *I*4/*mcm* [33].

However, examination of the high-resolution backscattering data above room temperature has shown three phase transitions. At 373 K, the basic (1 1 1) reflection also splits in two, and the doublet of the basic (200) reflection reverses its intensity. This is characteristic of an orthorhombic distortion. As the temperature increases further, e.g., at $T = 473$ K, the doublet of the basic (200) reflection merges into a single peak, but the splitting of the basic (1 1 1) reflection remains with the intensity ratio changing from ~1:1 to ~1:3. This structure is best described by a rhombohedral distortion. The rhombohedral structure continues until 1348 K, though the splitting of the basic (1 1 1) reflection becomes unobservable above about

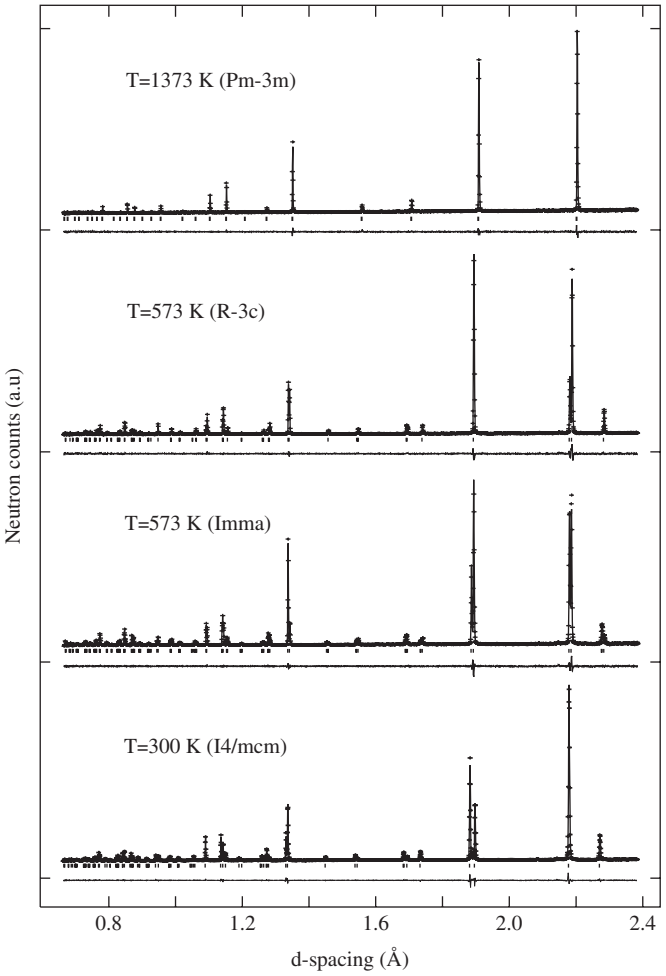

Fig. 2. Observed (crosses) and calculated (continuous line) high-resolution backscattering profiles of $CeAlO_3$ in the space groups *I*4/*mcm*, *Imma*, $R\bar{3}c$ and $Pm\bar{3}m$. Tick marks below indicate the positions of the allowed Bragg's reflections. The difference curves ($I_{obs.}-I_{cal.}$) are shown at the bottom.

1173 K. However, in this temperature range some super lattice reflections, e.g., at $d \approx 2.3$ Å (Fig. 2), persist, only to completely disappear at $T = 1373$ K. The neutron diffraction pattern is typically primitive cubic. As no additional super lattice reflections resulting from in-phase octahedral tilting (Fig. 2) were observed, we concluded that the structural changes in $CeAlO_3$ above room temperature correspond to the *I*4/*mcm* → *Imma*, *Imma* → $R\bar{3}c$ and $R\bar{3}c \rightarrow Pm\bar{3}m$ phase transitions.

Rietveld refinements carried out in the space groups[2] mentioned above yielded satisfactory results. Table 1 summarises the refined lattice parameters and atomic positions of $CeAlO_3$ in four different phases. Fig. 2 shows the plots of the observed and calculated profiles at some representative temperatures. Some selected interatomic distances are listed in Table 2.

[2]For easy comparison with the tetragonal structure, the space group *Ibmm*, instead of the standard *Imma*, was used with the *c*-axis as the longest one.

Table 1
Refined lattice parameters, atomic positions and thermal parameters of $CeAlO_3$ in the space groups $I4/mcm$, $Ibmm$, $R\bar{3}c$ and $Pm\bar{3}m$, respectively

T(K)	4.2	300	373	473	673	873	1073	1173	1323	1373	1423
Space group	$I4/mcm$	$I4/mcm$	$Ibmm$	$R\bar{3}c$	$R\bar{3}c$	$R\bar{3}c$	$R\bar{3}c$	$R\bar{3}c$	$R\bar{3}c$	$Pm\bar{3}m$	$Pm\bar{3}m$
a (Å)	5.31001(1)	5.32358(1)	5.35834(3)	5.33946(2)	5.35152(2)	5.36428(2)	5.37769(2)	5.38462(2)	5.39614(21)	3.817880(7)	3.820115(7)
b (Å)			5.33759(2)								
c (Å)	7.59984(3)	7.58849(4)	7.53647(3)								
α(°)				60.167(1)	60.134(1)	60.098(1)	60.062(1)	60.044(1)	60.004(4)		
Al	4*c* (0,0,0)		4*a* (0,0,0)	2*b* (0,0,0)						1*a* (0,0,0)	
U^*_{iso}	1.34(4)	0.96(3)	1.06(3)	1.06(3)	1.26(3)	1.45(3)	1.63(4)	1.77(4)	1.81(4)	1.90(4)	1.97(4)
Ce	4*b* (1/2,0,1/4)		4e (*x*,0,1/4)	2*a* (1/4,1/4,1/4)						1*b* (1/2,1/2,1/2)	
x			0.4996(3)								
U^*_{iso}	1.04(3)	0.95(3)	1.11(3)	1.22(3)	1.57(3)	1.86(3)	2.27(3)	2.46(3)	2.67(4)	2.77(4)	2.92(4)
O(1)	4*a* (0,0,1/4)		4e (*x*,0,1/4)	6e (*x*,1/2-*x*,1/4)		3d (1/2,0,0)					
X			0.0429(2)	0.78375(8)	0.78107(7)	0.77807(8)	0.77354(9)	0.77051(9)	0.76202(17)		
U^*_{iso}	1.20(3)	1.17(3)	1.20(4)	1.20(4)	1.78(2)	2.21(2)	2.67(2)	2.97(2)	3.24(2)	3.48(3)	3.57(3)
O(2)	8 h (*x*,1/2+*x*,0)		8 g (1/4,1/4,*z*)								
x	0.28531(7)	0.28119(7)									
z			−0.02158(9)								
U^*_{iso}	1.21(2)	1.05(2)	1.26(2)								
R_{wp} (%)	4.92	5.73	5.66	6.06	5.50	5.58	5.52	5.58	5.36	5.44	5.36
R_p (%)	3.96	4.75	4.95	5.25	4.61	4.71	4.47	4.52	4.32	4.32	4.27

$U^*_{iso} = U_{iso} \times 100$.

4. Discussion

The present high-resolution powder neutron diffraction study has confirmed that the structure of $CeAlO_3$ at room temperature is tetragonal, crystallising with a super cell instead of a primitive one. The tetragonal distortion is readily explained by the cooperative tilt of AlO_6 octahedra about the primitive four-fold $[001]_p$-axis resulting in the space group $I4/mcm$. The tilting angle at room temperature is about 7.1°. Due to octahedral tilting, the a-axis shrinks, the reduced c_r/a_r ratio becoming 1.008. The octahedral tilting changes the 12 Ce–O bond distances into four short, four medium and four long ones (Table 2). On the other hand, the change of the Al–O bond lengths is insignificant. Below room temperature, no phase transition was observed except a gradual increase of the tetragonal distortion. At 4 K, the tilting angle is about 8.1° with a reduced c_r/a_r ratio of 1.012.

Above room temperature, the tetragonal structure does not change directly into the primitive cubic as was anticipated; instead, it turns, e.g., at 373 K, into an orthorhombic structure with the space group *Imma*. This structure is obtained by octahedral tilting about the primitive two-fold $[1\,1\,0]_p$-axis with a tilting angle of about 6.9° at 373 K. This distortion results in seven shorter and five longer Ce–O distances (Table 2). Again, the Al–O bond distances change very little. The tilting about the two-fold $[1\,1\,0]_p$-axis shortens the c-axis leading to a ratio $c_r/a_r(b_r) < 1$.

As the temperature increases further, the rhombohedral $R\bar{3}c$ structure appears, e.g., at 473 K. This structure corresponds to tilting of the octahedra arround the primitive three-fold $[1\,1\,1]_p$-axis. This is just the structure of $LnAlO_3$ (Ln = La, Pr and Nd) at room temperature. In the rhombohedral phase, three short, six medium and three long Ce–O bonds occur (Table 2). On the other hand, tilting does not change the Al environment significantly. The rhombohedral structure persists till 1348 K. Above about 1373 K, the structure of $CeAlO_3$ becomes primitive cubic. Across the $R\bar{3}c \rightarrow Pm\bar{3}m$ phase transition, no discontinuous cell volume change is observed (Fig. 3). On the other hand, the tilting angle gradually decreases with increasing temperature (Fig. 4), indicating the approach to the cubic phase. Given that the same phase transition in $LnAlO_3$ (Ln = La, Pr and Nd) was ascribed to be continuous [19], we have estimated the transition temperature by choosing the tilting angle (φ) as the order parameter and fitting its variation with temperature (T) using the formula: $\varphi = A(T_c - T)^{\beta}$, where T_c is the transition temperature, and β is termed the "critical exponent". The experimentally fitted values are: $T_c = 1371$ K with $\beta = 0.35$ and $A = 0.52$ (Fig. 4). The T_c-value obtained falls well within the experimentally observed transition temperature range, i.e., between 1348 and 1373 K. However, the calculated β-value is not the expected one, neither for a mean field second-order transition ($\beta = 0.5$) nor for a tricritical transition ($\beta = 0.25$).

Table 2
Selected interatomic distances (Å) in $CeAlO_3$

T (K)	4.2	300	373	473	1373
Space group	$I4/mcm$	$I4/mcm$	$Ibmm$	$R\bar{3}c$	$Pm\bar{3}m$
Al–O(1)	1.89988(1) 2 ×	1.89712(1) 2 ×	1.8981(1) 2 ×	1.8987(4) 6 ×	1.90894 6 ×
Al–O(2)	1.89594(8) 4 ×	1.89676(7) 4 ×	1.89778(6) 4 ×		
Ce–O(1)	2.65490(1) 4 ×	2.66179(1) 4 ×	2.447(2)	2.4958(4) 3 ×	2.69965 12 ×
			2.6785(2) 2 ×	2.67584(3) 6 ×	
			2.911(2)	2.8571(4) 3 ×	
Ce–O(2)	2.4917(4) 4 ×	2.5125(4) 4 ×	2.5583(9) 4 ×		
	2.8635(4) 4 ×	2.8427(4) 4 ×	2.7853(9) 4 ×		

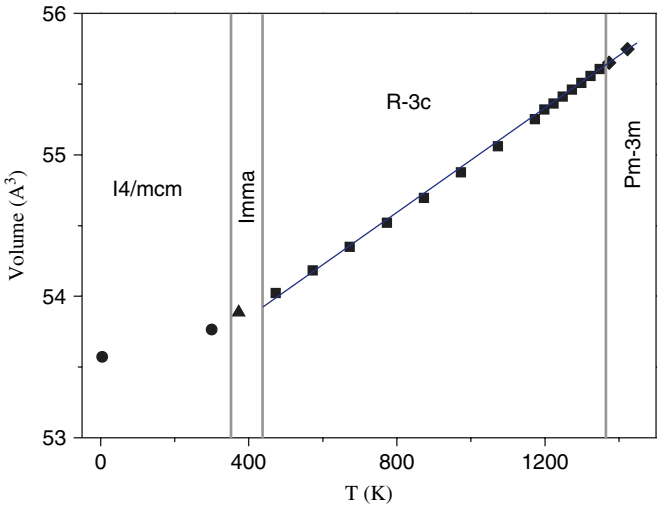

Fig. 3. Variation of the reduced cell volume as the function of temperature in $CeAlO_3$. Note that the lines that separate the $I4/mcm$ and $Imma$ phases and the $Imma$ and $R\bar{3}c$ phases are not experimentally determined transition temperatures but for visualisation purpose.

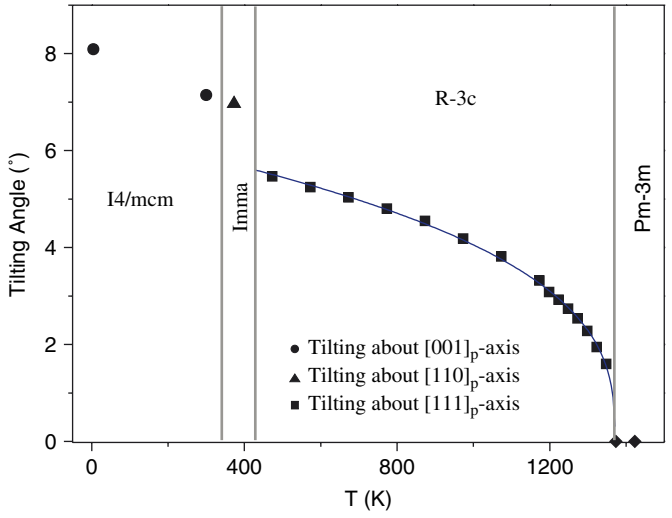

Fig. 4. Temperature dependence of the octahedral tilting angles in $CeAlO_3$. The continuous line in rhombohedral phase region is the fit to the expression: $\varphi = A(T_c - T)^{\beta}$ with fitted values of $T_c = 1371$ K, $\beta = 0.35$ and $A = 0.52$ (see also text). Note that the lines that separate the $I4/mcm$ and $Imma$ phases and the $Imma$ and $R\bar{3}c$ phases are not experimentally determined transition temperatures but for visualisation purpose.

Nevertheless, we have previously observed similar behaviour in $BaTbO_3$ ($\beta = 0.35$) [10] for the corresponding $I4/mcm \rightarrow Pm\bar{3}m$ phase transition. Interestingly, fitting the tilting angle of rhombohedral $LaAlO_3$ using the refined oxygen coordinates given in Ref. [19], we obtained a β-value of 0.36. Obviously, these continuous phase transitions have common features.

From the discussion given above, the phase sequence in $CeAlO_3$—with decreasing temperature—is: $Pm\bar{3}m \rightarrow R\bar{3}c \rightarrow Imma \rightarrow I4/mcm$. Of particular interest is that all three simple tilt systems, i.e., $(a^-a^-a^-)$, $(a^0b^-b^-)$ and $(a^0a^0c^-)$, have been observed. Here the $R\bar{3}c \rightarrow Imma$ and $Imma \rightarrow I4/mcm$ transitions must be the first-order ones [4]. It is interesting to compare this phase sequence with the others known in perovskites. As was mentioned in the introduction, A-cation driven phase transitions in ABO_3 perovskites usually follow the sequence of either $Pm\bar{3}m \rightarrow I4/mcm \rightarrow Imma \rightarrow Pnma$ or $Pm\bar{3}m \rightarrow R\bar{3}c \rightarrow Imma \rightarrow Pnma$, though the structure at lower temperatures has also been reported to have the space group $I2/m$ instead of $Pnma$ (see discussion below). Inspecting these sequences, some distinct features can be noticed. For instance, the cubic space group $Pm\bar{3}m$ changes into its subgroups: either $I4/mcm$ (tilt system $(a^0b^0c^-)$) or $R\bar{3}c$ (tilt system $(a^-a^-a^-)$); the immediate transition to the space group $Imma$ (tilt system $(a^0b^-b^-)$) is, apparently unknown. On the other hand, neither $I4/mcm$ nor $R\bar{3}c$ transforms directly into possible subgroups; both go via the space group $Imma$ to the space group $Pnma$ (tilt system $(a^+b^-b^-)$). Why any perovskite would follow such peculiar pathways does not seem to be well understood. However, examining the nature of the phase transitions as discussed by Howard and Stokes in their group theoretical study [4], one clear condition seems to exist: the transition from one space group into a subgroup seems to be possible only if the associated phase transition is continuous. However, between different subgroups a first-order phase transition may occur. For example, the $Pm\bar{3}m \rightarrow Imma$ transition is required by Landau theory to be of the first order [4], and it does not occur in perovskites. Also, since the space group $Pnma$ is a subgroup of neither $I4/mcm$ nor $R\bar{3}c$, perovskites crystallising in those space groups would first undergo a first-order transition to $Imma$, enabling the further

continuous transition to *Pnma*. Nevertheless, without theoretical confirmation, it is as yet unclear whether this condition may indeed account for the phase sequences observed.

In common perovskites the transition from *Imma* to *I*4/*mcm* occurs on an increase in temperature. In $CeAlO_3$ this transition occurs at decreasing temperatures. A simple *A*-cation driven mechanism cannot account for this anomaly. The presence of the tetragonal structure over a wide temperature range may have an electronic origin as the Ce(III) ion contains one 4*f*-electron. The La(III) counterpart, which does not have a 4*f*-electron, does not show the tetragonal phase at all [19]. The fact that the *Imma* → *I*4/*mcm* phase transition in $CeAlO_3$ is likely to be driven by the electronic structure of Ce(III) may seen too from the phases in the series of $Ce_{1-x}La_xAlO_3$. In this case, as La-substitution depopulates the 4*f*-electron at the *A*-site, one would expect that the tetragonal structure ceases to exist at certain doping level. Indeed, our preliminary results have shown that this occurs already at the *x*-value of about 0.1. In particular, we also observed the orthorhombic *Imma* structure in the compounds of the intermediate compositions before the occurrence of the rhombohedral $R\bar{3}c$ structure at higher degrees of La-substitution ($x \approx 0.5$). Details will be published elsewhere.

It is interesting to note that a similar structural behaviour has been observed in $PrAlO_3$ more than 30 years ago. This perovskite has the rhombohedral $R\bar{3}c$ structure at room temperature, and undergoes two phase transitions, near 205 and 150 K, respectively [35]. The first transition to an orthorhombic structure has been identified by Megaw [36] as corresponding to the $R\bar{3}c$ → *Imma* phase transition. The structure that results from the second transition, though being universally recognised as pseudo-tetragonal [37,38], remains unclear. Moussa et al. [14] have studied the phase transitions in $PrAlO_3$ using a combination of high-resolution neutron powder diffraction and synchrotron X-ray powder diffraction techniques. They proposed that the near 150 K phase transition corresponds to an orthorhombic (*Imma*) → monoclinic (*I*2/*m*) transition, which is continuous. Even so, their synchrotron data at 20 K show a virtually tetragonal metric. More recently, Carpenter et al. [15] have, using high-resolution time-of-flight neutron powder diffraction, investigated the strain mechanism through successive phase transitions in $PrAlO_3$. From the analysis of peak profiles close to the transition temperature, they confirmed the 150 K phase transition being *Imma* → *I*2/*m*. They also carried out refinements, using their 4.2 K neutron data, in both *I*4/*mcm* and the *I*2/*m* models. The tetragonal space group was rejected as it resulted in a poor agreement factor (R_{wp}). To see whether the proposed *I*2/*m* model might be compatible with the structure of $CeAlO_3$ at room temperature and below, we refined the structure at 4.2 K, using our data, in the monoclinic space group as well. While a comparable but somewhat higher agreement factor was obtained ($R_{wp} = 4.98\%$), the refined oxygen positions showed standard deviations being roughly 10 times higher compared to the refinement in *I*4/*mcm*. Also the refined lattice parameters, $a = 5.3412(1)$ Å, $b = 7.5093(2)$ Å, $c = 5.3432(2)$ Å and $\beta = 90.683°$, are very close to a tetragonal metric except for the large monoclinic angle. Considering further that the tilting of the AlO_6 octahedra in a monoclinic model is practically dominated by one tilt, being 7.6° vs. 1.0°, the space group *I*2/*m* clearly failed to model the structure of $CeAlO_3$.

It is unclear whether the phase transitions in $CeAlO_3$ and $PrAlO_3$ have the same mechanism given their similar electronic configurations and the close similarity of the low-temperature structures. In particular, whether the observed phase sequences of $Pm\bar{3}m \rightarrow R\bar{3}c \rightarrow Imma \rightarrow I4/mcm$ and $Pm\bar{3}m \rightarrow R\bar{3}c \rightarrow Imma \rightarrow I2/m$ are both valid for ABO_3-type perovskites remains to be clarified. As was discussed before, the *Imma* → *I*4/*mcm* phase transition with decreasing temperature does not usually occur in perovskites, which may suggest an electronic origin. On the other hand, the *Imma* → *I*2/*m* transition would obey group–subgroup relations [4]. Nevertheless, in many perovskites the *Imma* structure transforms to the subgroup *Pnma* at low temperatures instead of to *I*2/*m*. As was explained by Woodward [39], the orthorhombic tilt system ($a^+b^-b^-$) (*Pnma*) provides the best balance between maximising the coulomb attraction while minimising repulsive ion–ion interactions, if large tilting angles are required. As the tilt system ($a^0b^-c^-$) (*I*2/*m*) is, actually, intermediate between the tilt system ($a^0b^-b^-$) (*Imma*) and ($a^0a^0c^-$) (*I*4/*mcm*), i.e., when two tilting angles are either equal or one tilting angle is zero, it is questionable whether a perovskite would adopt the *I*2/*m* space group. In fact, in the ABO_3-type perovskites, only $BaPbO_3$ has, besides $PrAlO_3$, once been reported to have this structure [12,13,40]. But the monoclinic structure in $BaPbO_3$ is disproved by a recent high-resolution neutron powder diffraction study [10], which showed that the line broadening of some diffraction lines that has been attributed to the monoclinic distortion is likely due to the presence of micro twins. In this regard, the structure of $PrAlO_3$ at low temperature necessitates a closer examination to see whether it is indeed monoclinic or the correct space group is tetragonal—*I*4/*mcm*—by considering the possibly similar anisotropic line broadening effect.

In conclusion, we have investigated the structure of $CeAlO_3$ in a wide temperature range. The tetragonal *I*4/*mcm* structure at room temperature, once reported from X-ray powder diffraction data, is firmly confirmed, and no phase transition is observed below room temperature till 4.2 K. On the other hand, $CeAlO_3$ undergoes the successive phase transitions to the orthorhombic *Imma* structure (e.g., $T = 373$ K), the rhombohedral $R\bar{3}c$ structure (e.g., 473 K) and finally the cubic $Pm\bar{3}m$ structure at about above 1373 K. The phase sequence, $Pm\bar{3}m \rightarrow R\bar{3}c \rightarrow Imma \rightarrow I4/mcm$, occurring in $CeAlO_3$, is unique in the ABO_3-type perovskites.

Acknowledgments

The authors are indebted to Dr. K.S. Knight and Mr. R. Haynes of the ISIS facility for the collection of neutron powder diffraction data, and to Mr. M. Biglari for preparing samples of $Ce_{1-x}La_xAlO_3$. Financial support from the Netherlands Organisation for Scientific Research (NWO) for this work is gratefully acknowledged.

Note added

After submitting this paper we learnt from one of the reviewers the works of L. Vasylechko et al. on $CeAlO_3$ using high-resolution synchrotron X-ray diffraction technique (see Ref. [41] and the attached PDF's and web addresses). In particular, they identified the phase sequence in $CeAlO_3$ being: $I4/mcm \rightarrow Imma \rightarrow R\bar{3}c \rightarrow Pm\bar{3}m$. Our results are in agreement with their findings.

References

[1] H.D. Megaw, Nature 155 (1945) 484.
[2] A.M. Glazer, Acta Crystallogr. B 28 (1972) 3384.
[3] A.M. Glazer, Acta Crystallogr. A 31 (1975) 756.
[4] C.J. Howard, H.T. Stokes, Acta Crystallogr. B 54 (1998) 782.
[5] B.J. Kennedy, C.J. Howard, Phys. Rev. B 59 (1999) 4023.
[6] C.J. Howard, K.S. Knight, B.J. Kennedy, E. Kisi, J. Phys.: Condens. Matter 12 (2000) L677.
[7] B.J. Kennedy, C.J. Howard, B.C. Chakoumakos, Phys. Rev. B 60 (1999) 2972.
[8] B.J. Kennedy, B.A. Hunter, Phys. Rev. B 58 (1998) 653.
[9] B.J. Kennedy, B.A. Hunter, J.R. Hester, Phys. Rev. B 65 (2002) 224103.
[10] W.T. Fu, D. Visser, K.S. Knight, D.J.W. IJdo, J. Solid State Chem. 177 (2004) 1667.
[11] K.S. Knight, Solid State Ionics 74 (1994) 109.
[12] S.A. Ivanov, S.-G. Eriksson, R. Tellgren, H. Rundlof, Mater. Sci. Forum 378–381 (2001) 511.
[13] S.M. Moussa, B.J. Kennedy, T. Vogt, Solid State Commun. 119 (2001) 549.
[14] S.M. Moussa, B.J. Kennedy, B.A. Hunter, C.J. Howard, T. Vogt, J. Phys.: Condens. Matter 13 (2001) L203.
[15] M.A. Carpenter, C.J. Howard, B.J. Kennedy, K.S. Knight, Phys. Rev. B 72 (2005) 024118.
[16] W.T. Fu, D. Visser, D.J.W. IJdo, Solid State Commun. 134 (2005) 647.
[17] P.D. Dernier, R.G. Maines, Mater. Res. Bull. 6 (1971) 433.
[18] M. Marezio, P.D. Dernier, J.P. Remeika, J. Solid State Chem. 4 (1972) 11.
[19] C.J. Howard, B.J. Kennedy, B.C. Chakoumakos, J. Phys.: Condens. Matter 12 (2000) 349.
[20] A. Bombik, B. Lesniewska, J. Mayer, A. Oles, A.W. Pacyna, J. Przewoznik, J. Magn. Magn. Mater. 168 (1997) 139.
[21] A.A. Levin, Kristallografiya 37 (1992) 1020.
[22] W.T. Fu, H.W. Zandbergen, D.J.W. IJdo, Mater. Res. Bull. 39 (2004) 909.
[23] R. Diehl, G. Brandt, Mater. Res. Bull. 10 (1975) 85.
[24] A. Piras, A. Trovareli, G. Dolcetti, Appl. Catal. 28 (2000) 77.
[25] W.H. Zachariasen, Acta Crystallogr. 2 (1949) 388.
[26] A.C. Tas, M. Akinc, J. Am. Ceram. Soc. 77 (1994) 2961.
[27] R.S. Roth, J. Res. NBS 58 (1957) 75.
[28] Y.S. Kim, Acta Crystallogr. B 24 (1968) 295.
[29] A.I. Leonov, A.V. Andreeva, V.E. Shavaiko-Shavaikoviskii, E.K. Keler, Izv. Akad. Nauk SSSR, Neorg. Mater. 2 (1966) 517.
[30] V.M. Egorov, Y.M. Baikov, N.K. Kartenko, B.T. Melekh, Y.N. Filin, Phys. Solid State 40 (1998) 2109.
[31] A.I. Shelykh, B.T. Melekh, Phys. Solid State 45 (2003) 248.
[32] M. Tanaka, T. Shishido, H. Horiuchi, N. Toyota, D. Shindo, T. Fukuda, J. Alloys Compd. 192 (1993) 87.
[33] W.T. Fu, D.J.W. IJdo, J. Solid State Chem. 177 (2004) 2973.
[34] A. C. Larson, R. B. Von Dreele, GSAS General Structure Analysis System, Report LAUR 86-748. Los Alamos National Laboratory, Los Alamos, NM, 1986.
[35] E. Cohen, L.A. Risberg, W.A. Nordland, R.D. Burbank, R.C. Sherwood, L.G. Van Uitert, Phys. Rev. 186 (2) (1969) 476.
[36] H.D. Megaw, Crystal Structures—A Working Approach, W.B. Saunders, Philadelphia, 1973.
[37] P.T. Harley, W. Hayes, A.M. Perry, S.R.P. Smith, J. Phys. C: Solid State Phys. 6 (1973) 2382.
[38] R.J. Birgeneau, J.K. Kjems, G. Shirane, L.G. Van Uitert, Phys. Rev. B 10 (1974) 2512.
[39] P.M. Woodward, Acta Crystallogr. B 53 (1997) 44.
[40] H. Ritter, J. Ihringer, J.K. Maichle, W. Prandl, A. Hoser, A.W. Hewat, Z. Phys. B 75 (1989) 297.
[41] L.O. Vasylechko, A.O. Matkovskii, Bull. Lviv Polytech. Natl. Univ., Electronics, 514, 2004, 33, 52, PDF cards NN 55-890, 55-889, 55-676, 55-961 and 55-633 http://www-hasylab.desy.de/science/annual_reports/2002_report/index.html, http://www-hasylab.desy.de/science/annual_reports/2003_report/index.html.